PRAMANA — journal of physics

Vol. 82, No. 3
March 2014
pp. 585–605

Long term performance evaluation of the TACTIC imaging telescope using ∼400 h Crab Nebula observation during 2003–2010

A K TICKOO*, R KOUL, R C RANNOT, K K YADAV, P CHANDRA, V K DHAR, M K KOUL, M KOTHARI, N K AGARWAL, A GOYAL, H C GOYAL, S KOTWAL, N KUMAR, P MARANDI, K VENUGOPAL, K CHANCHALANI, N BHATT, S BHATTACHARYYA, C BORWANKAR, N CHOUHAN, S R KAUL, A K MITRA, S SAHAYNATHAN, M SHARMA, K K SINGH and C K BHAT

Astrophysical Sciences Division, Bhabha Atomic Research Centre, Mumbai 400 085, India
*Corresponding author. E-mail: aktickoo@barc.gov.in

MS received 28 May 2013; revised 21 November 2013; accepted 25 November 2013
DOI: 10.1007/s12043-014-0707-8; ***e*Publication:** 7 March 2014

Abstract. The TeV atmospheric Cherenkov telescope with imaging camera (TACTIC) γ-ray telescope has been in operation at Mt. Abu, India since 2001 to study TeV γ-ray emission from celestial sources. During the last 10 years, apart from consistently detecting a steady signal from the Crab Nebula above ∼1.2 TeV energy, at a sensitivity level of $\sim 5.0\sigma$ in ∼25 h, the telescope has also detected flaring activity from Mrk 421 and Mrk 501 on several occasions. Although we used Crab Nebula data partially, in some of the reported results, primarily for testing the validity of the full data analysis chain, the main aim of this work is to study the long term performance of the TACTIC telescope by using consolidated data collected between 2003 and 2010. The total on-source data, comprising ∼402 h, yields an excess of $\sim(3742\pm192)$ γ-ray events with a statistical significance of $\sim 19.9\sigma$. The off-source data, comprising ∼107 h of observation, is found to be consistent with a no-emission hypothesis, as expected. The resulting γ-ray rate for the on-source data is determined to be $\sim(9.31\pm0.48)\,\mathrm{h}^{-1}$. A power law fit ($\mathrm{d}\Phi/\mathrm{d}E = f_0 E^{-\Gamma}$) with $f_0 \sim (2.66 \pm 0.29) \times 10^{-11}$ cm^{-2} s^{-1} TeV^{-1} and $\Gamma \sim 2.56 \pm 0.10$ is found to provide reasonable fit to the inferred differential spectrum within statistical uncertainties. The spectrum matches reasonably well with that obtained by other groups. A brief summary of the improvements in the various subsystems of the telescope carried out recently, which has resulted in a substantial improvement in its detection sensitivity (viz., $\sim 5\sigma$ in an observation period of ∼13 h as compared to ∼25 h earlier) are also presented in this paper. Encouraged by the detection of strong γ-ray signals from Mrk 501 and Mrk 421 on several occasions, there is considerable scope for the TACTIC telescope to monitor similar TeV γ-ray emission activity from other active galactic nuclei on a long-term basis.

Keywords. Cherenkov imaging technique; TeV atmospheric Cherenkov telescope with imaging camera telescope; Crab Nebula observation.

PACS Nos 95.55.Ka; 95.85.Pw; 29.40.Ka

1. Introduction

Ground-based imaging atmospheric Cherenkov telescopes have become the most efficient instruments for the observation of γ-rays in the TeV energy range [1–3]. The γ-rays trace back to cosmic accelerators which may also be responsible for the creation and acceleration of the charged cosmic rays, and are expected to come from a wide variety of cosmic objects within and outside our galaxy. Studying this radiation in detail can yield valuable and quite often, unique information about the unusual astrophysical environment characterizing these sources, as also on the intervening intergalactic space [4–6]. The Cherenkov imaging technique was applied for the first time in 1988–1989 by the Whipple Collaboration to detect steady γ-ray emission from the Crab Nebula using a 10 m reflector with a 37-pixel photomultiplier tube camera [7]. Another important development in the field was the application of stereoscopic imaging, proposed by the HEGRA [8] group, which proved that the information available from multiple telescopes, located within the same Cherenkov light pool, can dramatically improve the sensitivity of the technique. It was the landmark development of these two methods that revolutionized the field of ground-based very high-energy (VHE) γ-ray astronomy.

A Cherenkov imaging telescope records the spatial distribution of the photons in the image plane (called the Cherenkov image) and a close-packed array of fast photomultiplier tubes is used for recording this distribution (also called the imaging camera with individual PMTs as its pixels). The appearance of the recorded image depends upon a number of factors like the nature and the energy of the incident particle, the arrival direction and the impact point of the particle trajectory on the ground. Segregating the very high-energy γ-ray events from their cosmic ray counterpart is achieved by exploiting the subtle differences that exist in the two-dimensional Cherenkov image characteristics (shape, size and orientation) of the two event species. Gamma-ray events give rise to shower images which are preferentially oriented towards the source position in the image plane. Apart from being narrow and compact in shape, these images have a cometary shape with their light distribution skewed towards their source position in the image plane and become more elongated as the impact parameter increases. On the other hand, hadronic events give rise to images that are, on an average, broader and longer and are randomly oriented within the field of view of the camera. For each image, which is essentially elliptical in shape, Hillas parameters [9,10] are calculated to characterize its shape and orientation. The parameters are obtained using moment analysis and are defined as: LENGTH – The rms spread of light along the major axis of the image (a measure of the vertical development of the shower); WIDTH – The rms spread of light along the minor axis of the image (a measure of the lateral development of the shower); DISTANCE – The distance from the centroid of the image to the centre of the field of view; ALPHA (α) – The angle between the major axis of the image and a line joining the centroid of the image to the position of the source in the focal plane; SIZE – Sum of all the signals recorded in the clean Cherenkov image; FRAC2 – The degree of light concentration as determined from the ratio of the two largest PMT signals to sum of all signals

(also referred to as Conc.). In the pioneering work of the Whipple Observatory [7], only one parameter (AZWIDTH) was used in selecting γ-ray events. Later, the technique was refined to supercuts/dynamic supercuts procedure where cuts based on the WIDTH and LENGTH of the image as well as its orientation are used for segregating the γ-rays from the background cosmic rays [11]. Modern instruments use multiple telescopes to image the air-shower from different viewing angles for improved reconstruction of γ-ray direction and rejection of cosmic-ray background. The stereoscopic method also allows rejection of triggers caused by cosmic-ray secondary muons. Telescope systems such as HESS [12] provide an angular resolution for single γ-rays of 3 arc-min to 6 arc-min, a γ-ray energy resolution of around 15% and an unprecedented sensitivity with cosmic-ray rejection factor of more than 99.9%.

The Crab supernova remnant (SNR) is a very well-studied object, with detailed observations across the entire accessible energy spectrum. At a distance of $\sim$2000 pc, it is a prototypical centre-filled SNR, or plerion. The Crab pulsar lies within the supernova remnant and has rotational period of $\sim$33 m s with a spin-down luminosity of $\sim 4.6\times10^{38}$ erg s^{-1}. The total energy available from the pulsar to power the surrounding synchrotron nebula is of the order of 10^{38} erg. The spectral energy distribution of the non-thermal nebula emission displays two components where, the low-frequency component is explained by synchrotron radiation of high-energy electrons spiraling in the magnetic field of the nebula [13] and the higher frequency component is attributed to inverse Compton scattering of lower energy synchrotron photons by these electrons. Although the inverse Compton mechanism gives a good description of the observed energy spectrum between $\sim$500 GeV and $\sim$10 TeV, other processes may also partially contribute to the VHE γ-ray emission. Pulsed emission from the pulsar has also been detected by MAGIC and VERITAS and the emission has been seen to extend up to well beyond 100 GeV [14,15]. Due to high flux from the source as compared to other known TeV sources, and its constant flux, it is conventionally used as a standard candle in the field of VHE astronomy. However, multiple day-scale flaring events at energies below 1 GeV have been detected by the Large Area Telescope on board the Fermi Gamma-ray Space Telescope [16,17] and evidence for an enhanced flux during flare states by ARGO-YBJ [18,19] have been reported. Measurements from Cherenkov imaging telescope do not support these results, but are not necessarily in conflict, because of the differing duty cycles.

The paper is organized in the following manner. Section 2 will cover some important design features of the telescope. Observation details on the Crab Nebula and performance evaluation on the basis of zenith angle dependence of the cosmic-ray rate will be presented in §3. The procedure for extracting γ-ray signal from the α plot and results obtained on Crab Nebula will be presented in §4. Section 5 will cover the energy reconstruction procedure and the energy spectrum of the Crab Nebula as measured by the TACTIC telescope. Performance evaluation on the basis of sensitivity estimates will be presented in §6. Recent upgradation and some important scientific objectives for continuing observations with TACTIC will be presented in §7 and in §8 we present our conclusions. Sufficient details about Cherenkov imaging technique and TACTIC telescope have also been presented in the paper so that the manuscript can be easily followed by researchers who are not experts in the field of ground-based very high-energy γ-ray astronomy.

2. TACTIC telescope

The TeV atmospheric Cherenkov telescope with imaging camera (TACTIC) γ-ray telescope [20] has been in operation at Mt. Abu (24.6°N, 72.7°E, 1300 m asl), a hill resort in Western India, for the last several years for studying TeV γ-ray emission from celestial sources. The photographs of the TACTIC imaging telescope and its back-end signal processing electronics are shown in figure 1. While the details of the instrumentation aspects of the telescope can be seen in [20], we shall present here only the main design features of the telescope. The TACTIC light-collector with a collection area of $\sim$9.5 m^2 uses 34 front-face aluminium-coated, glass spherical mirrors of 60 cm diameter each with the following characteristics: (i) focal length $\sim$400 cm, (ii) surface figure $\sim \leq$ 800 nm, (iii) reflection coefficient $>$80% at a wavelength of $\sim$400 nm and (iv) thickness 20 mm–40 mm. The point-spread function has a FWHM of $\sim$ 0.185° ($\equiv$12.5 mm) and $D_{90} \sim$ 0.34° ($\equiv$22.8 mm). Here, D_{90} is defined as the diameter of a circle, concentric with the centroid of the image, within which 90% of reflected rays lie. Other details regarding performance evaluation of the light collector design can be seen in [21].

The telescope deploys a 349-pixel imaging camera, with a uniform pixel resolution of $\sim$ 0.31° and a $\sim$ 5.9°$\times$5.9° field-of-view, to record atmospheric Cherenkov events produced by an incoming cosmic-ray particle or a γ-ray photon. The 0.3° resolution imaging camera has been designed as a square grid and uses 19 mm diameter photomultiplier tubes (ETL-9083 UVB). The bialkali photocathode has a maximum quantum efficiency of $\sim$27% at 340 nm and the use of UV glass for the window has enhanced its sensitivity in the 280–300 nm wavelength band. The 10-stage linear focussed photomultiplier tube (PMT) has a rise time of $\sim$1.8 ns. A low current zener diode-based voltage divider

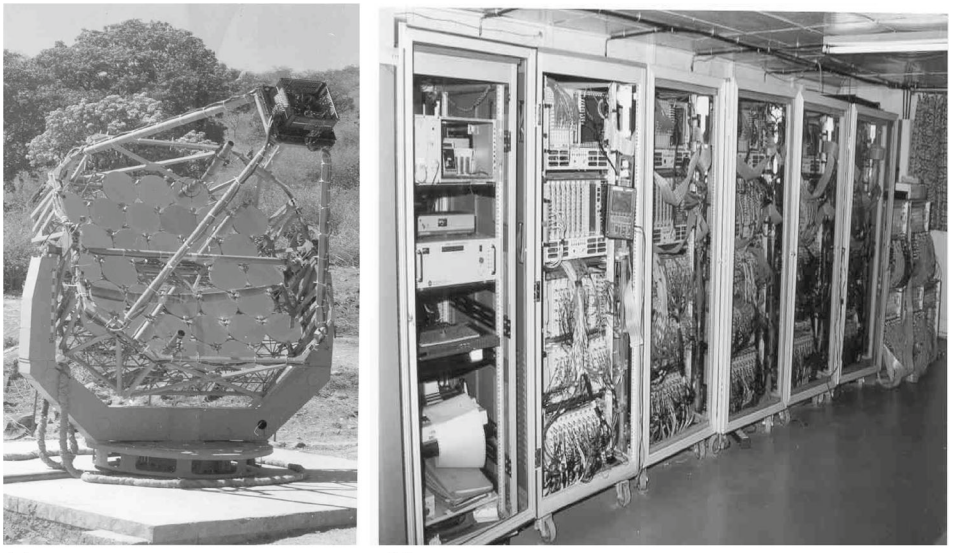

(a) (b)

Figure 1. (**a**) Photograph of the 349-pixel TACTIC imaging telescope. (**b**) Indigenously developed back-end signal processing electronics used in the telescope.

network (VDN) is used with the PMT operated in the grounded anode configuration with a negative voltage in the 1000–1400 V range. The circular entry and circular exit compound parabolic concentrators (CPC), made of SS-304, are placed on top of the PMTs to ensure better light collection efficiency. Some of the important geometrical parameters of the CPCs used in the TACTIC telescope camera are the following: entry aperture ∼21.0 mm; exit aperture ∼15.0 mm; acceptance angle ∼45.58° and height ∼17.6 mm. The light collection of the CPC, which includes both the geometrical collection efficiency and the reflectivity of the surface, was experimentally measured to be ∼65%.

The innermost 240 pixels (16 × 16 matrix) or 121 pixels (11 × 11 matrix) are used for generating the event trigger, based on a predecided trigger criterion which is either nearest neighbour pairs (NN2) or nearest neighbour triplets (NN3). Apart from generating the prompt trigger with a coincidence gate width of ∼18 ns, the trigger generator has a provision for producing a chance coincidence output based on $^{12}C_2$ combinations from various groups of closely spaced 12 channels. Design and implementation details of the multimodule trigger generator are discussed in a study [22]. The data acquisition and control system of the telescope [23] have been designed around a network of PCs running the QNX real-time operating system and is handled by a network of three personal computers. While one PC is used to monitor the scaler rates and control the high voltage (HV) to the photomultipliers, the other PC handles the acquisition of the event and calibration data and the programming of the TACTIC trigger generator (TTG) modules. These two front-end PCs, referred to as the rate stabilization node and the data acquisition node respectively, along with a master node form the multinode data acquisition and control network of the TACTIC imaging telescope. The same network is extended to two more LINUX-based PCs which are used for online data analysis and archiving. An event handler module controls the whole process of data acquisition and also provides the link between the TACTIC hardware and the application software. The event handler accepts the atmospheric Cherenkov events, calibration and chance trigger outputs from various TTG modules and interrupts the front end data acquisition node. The system acquires 349 channel CDC data for the trigger selected atmospheric Cherenkov events, relative calibration flashes generated by the calibration LED and sky pedestal events. The high voltage and scaler data are also logged continuously, though at a much lower frequency. At event occurrence the event handler also generates a TTL output for latching the system clock and a 20 ns wide NIM pulse for gating the CDC modules. The triggered events are digitized by CAMAC-based 12-bit charge to digital converters (CDC) which have a full scale range of 600 pC. The relative gain of the photomultiplier tubes is monitored regularly once in 15 min by flashing a blue LED, placed at a distance of ∼1.5 m from the camera. Other details regarding hardware and software features of the data acquisition and control system of the telescope are discussed in [23].

The drive control system uses hybrid stepper motors, sequence generators and power amplifiers, 16-bit absolute shaft-encoders, programmable stepper motor controllers and a GPS clock. Two CAMAC-compatible, 24-bit input registers have been used to input telescope zenith and azimuth information to the drive system computer to enable its control software to work in a closed-loop configuration with absolute shaft encoders monitoring the azimuth and zenith angles of the telescope and the corresponding stepper motors providing the movement of its axes. The telescope has a

pointing and tracking accuracy of better than ±3 arc-min. The tracking accuracy is checked on a regular basis with the so-called 'point runs', where an optical star having its declination close to that of the candidate γ-ray source is tracked continuously for about 5 h. The point run calibration data are then incorporated in the analysis software so that appropriate corrections can be applied in an offline manner during data analysis.

Detailed Monte Carlo simulations have also been performed to optimize the trigger field of view and the topological trigger generation scheme [24]. The results of this study suggest that, for NN-2 trigger case with a single pixel threshold of ∼22 photoelectrons, γ-ray threshold energy of the telescope is ∼1.2 TeV at a typical zenith angle of 15°. For the same zenith angle and using NN-3 trigger with a single pixel threshold of ∼14 photoelectrons, the γ-ray threshold energy is found out to be again close to ∼1.2 TeV. While optimizing the topological trigger generation, it is also found that using a NN-2 trigger methodology is a better option than the NN-3 trigger configuration when a source needs to be observed at zenith angles of >25°. Procedure for generating the Monte Carlo simulated database and formalism for calculating effective collection areas, threshold energy and detection rates are given in [24].

With a 5σ sensitivity of detecting the Crab Nebula in ∼25 h of observation time, regular observations were taken on a number of potential γ-ray sources (viz., Mrk 421, Mrk 501, 1ES2344 + 514, PSR 0355 + 54, ON 231, H1426 etc.) during the last 10 years and the results of these observations have been presented in [25–30]. A brief summary of these observations and results obtained are also given in table 1. While some of these reported results use Crab Nebula data (viz., data for ∼101.44 h collected between Nov. 10, 2005 and Jan. 30, 2006), primarily for testing the validity of the data analysis chain including the energy estimation procedure, the main aim of this work is to study the long term performance of the TACTIC telescope by using consolidated data of ∼400 h collected between 2003 and 2010.

Table 1. Observation log and published results on various sources observed with TACTIC telescope during the period 2004 to 2010. The notation UL used in the table stands for upper limit.

Source name	Obs. period	Obs. time (h) On (Off)	Results	Reference
Mrk 421	Dec. 2005–Apr. 2006	201.7 (29.7)	Detection – 11.5σ	[25]
	Dec. 2006–Apr. 2007	122.7 (***)	Low state – UL	[26]
	Jan. 2008–May 2008	184.8 (***)	Detection – 9.7 σ	[26]
	Nov. 2009–May 2010	229.9 (***)	Detection – 12.1 σ	[27]
Mrk 501	Mar. 2005–May 2005	46.0 (***)	Low state – UL	[28]
	Feb. 2006–May 2006	66.8 (***)	Detection – 7.5 σ	[28]
1ES2344+514	Oct. 2004–Dec. 2004	30.4 (10.9)	Low state – UL	[29]
	Oct. 2005–Jan. 2006	31.5 (9.4)	Low state – UL	[29]
H1426+428	Mar. 2004–Apr. 2004	44.8 (***)	Low state – UL	[30]
	Mar. 2006–May 2006	18.4 (***)	Low state – UL	[30]
	Mar. 2007–June 2007	102.5 (***)	Low state – UL	[30]
Total	Mar. 2004–May 2010	1079.5 (50.0)	**********	***

3. Crab Nebula observations and data analysis

The TACTIC imaging element saw first light in March 1997 when it successfully detected γ-ray flaring activity from Mrk-501 [31] and since then it was regularly deployed for observing a number of γ-ray sources. Upgradation of its prototype 81-pixel camera was undertaken in two stages. In the first stage the camera was upgraded to 144 pixels and in the next stage of upgradation which took place during Jan. 1999–Dec. 2000, the final camera configuration of 349 pixels was attained. Observations on potential γ-ray sources, however, were continued during this period of upgradation phase whenever it became possible to do so. First successful detection of TeV γ-rays from the Crab Nebula was seen in the data collected by the telescope for $\sim$41.5 h between 19 January and 23 February 2001. The data were taken by using a NN-3 topological trigger with the innermost 240 pixels (15 $\times$ 16 matrix) of the camera participating in generating the event trigger. A statistically significant excess of $\sim 6.3\sigma$ was seen in the data with $\sim 447 \pm 71$ γ-ray like events.

Although we have been regularly observing the Crab Nebula since 2001, we shall use here on-source data for the following four observing spells: ON-0304 – 17 Dec. 2003–23 Feb. 2004; ON-0506 – 10 Nov. 2005–30 Jan. 2006; ON-0708 – 03 Nov. 2007–08 Mar. 2008 and ON-0910 – 25 Oct. 2009–17 Feb. 2010. For validating the procedure for calculating expected background in the γ-domain, we shall use off-source data for two observing spells: OFF-0304 – 16 Dec. 2003–23 Feb. 2004 and OFF-0708 – 01 Nov. 2007–04 Jan. 2008. The zenith angle covered during a given ON/OFF source run was limited to $\leq 45^\circ$. A major portion of the data has been collected with 121 pixels (11×11 matrix) participating in the trigger with either NN-2 or NN-3 trigger configuration and using a total of 225 pixels. Several standard data quality checks have been used to evaluate the overall system behaviour and the quality of the recorded data. These include conformity of the prompt coincidence rates with the expected zenith angle dependence, compatibility of the arrival times of prompt coincidence events with Poissonian statistics and the behaviour of the chance coincidence rate with time. The details of the observation log, after applying these data quality checks, are given in table 2.

A representative example of the behaviour of prompt coincidence rate as a function of zenith angle is shown in figure 2. The result shown in figure 2a is the analysis of the NN-2 trigger mode ON-0506 data collected for $\sim$101.04 h. The total data in this spell

Table 2. Spell-wise break up of the observation log of the Crab Nebula ON/OFF-source data.

Spell	Observing period	No. of nights	Observation time (h)	Trigger
ON-0304	17 Dec. 2003–23 Feb. 2004	36	104.28	NN3
ON-0506	10 Nov. 2005–30 Jan. 2006	42	101.04	NN2
ON-0708	03 Nov. 2007–08 Mar. 2008	41	105.16	NN3
ON-0910	25 Oct. 2009–17 Feb. 2010	32	91.50	NN3
All ON		151	401.98	–
OFF-0304	16 Dec. 2003–23 Feb. 2004	32	67.94	NN3
OFF-0708	01 Nov. 2007–04 Jan. 2008	24	39.22	NN3
All OFF		56	107.16	–

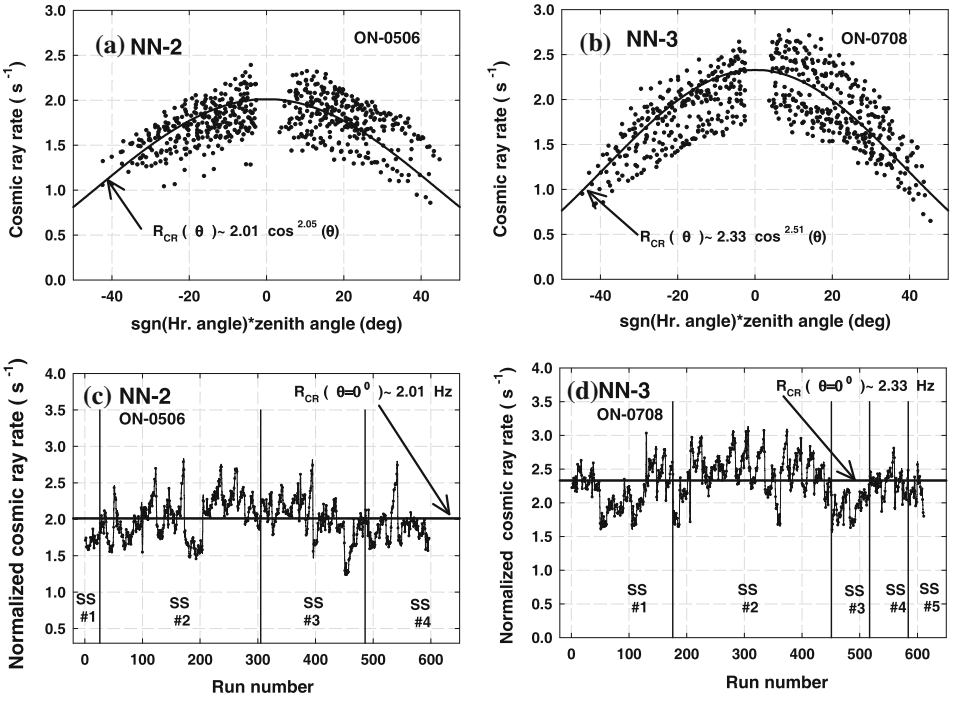

Figure 2. Measured cosmic-ray trigger rate as a function of zenith angle. (**a**) ON-0506 spell collected with NN-2 trigger configuration, (**b**) ON-0708 spell collected with NN-3 trigger configuration. Normalized cosmic-ray rate as a function of run number (**c**) ON-0506 spell and (**d**) ON-0708 spell. The segmentation of the data into various subspells, on the basis of one lunation period, are indicated by full vertical lines. The negative values of the zenith angle in (**a**) and (**b**) signify that the source being tracked is due east from zenith direction and the positive values signify directions which are due west.

have been divided into subspells, where each subspell corresponds to one lunation period. Each point in this plot represents a 10-min observation run and the event rate has been calculated by dividing the number of events recorded in 600 s. The behaviour of the measured values of cosmic-ray rate as a function of zenith angle for the ON-0708 data taken with NN-3 trigger mode is shown in figure 2b. In this case, the total data have been divided into five subspells. The corresponding Monte Carlo estimates (solid line), with $R_{\rm CR}(\theta) \sim 2.01(\cos\theta)^{2.05}$ Hz for NN-2 trigger and $R_{\rm CR}(\theta) \sim 2.33(\cos\theta)^{2.51}$ Hz for NN-3 trigger, are also shown in figures 2a and 2b, respectively. Detailed results of Monte Carlo simulations of γ-ray and cosmic-ray proton-induced extensive air showers as detected by the TACTIC atmospheric Cherenkov imaging telescope for optimizing its trigger field of view and topological trigger generation scheme can be found in [24].

Prior to the application of supercuts/dynamic supercuts analysis, the raw Cherenkov images recorded by the telescope need to be processed through the following steps: (a) pedestal subtraction, (b) image cleaning and (c) normalization of the PMT gains, a process also known as 'flat fielding'. The pedestal value for each PMT is determined by

artificially triggering the camera, thereby capturing CDC values in the absence of genuine input signal. Acquisition of the calibration data in this manner is called the sky pedestal run. An important step towards obtaining the clean image involves using the sky pedestal data so that the pixels which are not participating in a Cerenkov image can be removed. This ensures that maximum number of pixels which contain the genuine Cherenkov photons alone are retained. A standard method followed to obtain the clean image involves selecting a pixel to be part of the image if it has a signal above a certain threshold or is adjacent to such a pixel which has a signal above a lower threshold [32]. These two thresholds are referred to as the 'picture' and 'Boundary' thresholds, respectively. These thresholds are multiples of the RMS pedestal deviation, which the PMT signals must exceed to be considered part of the 'Picture' or 'Boundary'. All other pixels which do not satisfy this criterion are set to zero. A 'Picture' threshold of $\geq 6.5\sigma$ and a 'Boundary' threshold of $\geq 3.5\sigma$ have been used by us to select maximum number of PMTs with signal, while at the same time limiting the inclusion of PMTs with noise alone. The next step in the analysis is to account for the differences in the relative gains of the PMTs, a process known as the 'Flat Fielding'. This is determined by recording 2000 images using a pulsed light source in front of the camera surface. A fast blue LED with a light-diffusing medium in front of it has been used to ensure uniformity of the photon field across the camera surface.

4. Extracting the γ-ray signal by analysing α plot

After performing 'image cleaning' and 'flat fielding', the next step which needs to be followed in the data analysis is the image parametrization and event selection. The cleaned and flat fielded Cherenkov light images from each shower are analysed offline using a moment analysis technique. The derived image parameters are then used to distinguish candidate γ-ray events from the large background of cosmic-ray generated events. As already mentioned in §1, these parameters include LENGTH, WIDTH, DISTANCE, ALPHA(α), SIZE (S) and FRAC2. The standard dynamic supercut procedure [11] is then used to separate γ-ray like images from the background cosmic rays. The dynamic supercut γ-ray selection criteria used in the present analysis are the same as used in our previous work [33] and are the following: $0.11^\circ \leq \text{LENGTH} \leq (0.260 + 0.0265 \times \ln S)^\circ$, $0.06^\circ \leq \text{WIDTH} \leq (0.110 + 0.0120 \times \ln S)^\circ$, $0.52^\circ \leq \text{DISTANCE} \leq 1.27^\circ \cos^{0.88}\theta$, SIZE $\geq$ 450 d.c. (where 6.5 digital counts$\equiv$1.0 pe), ALPHA(α) $\leq 18^\circ$ and FRAC2 $\geq$ 0.35. It is important to emphasize here that the dynamic supercut γ-ray selection criteria used in the present analysis are the same which we had used in our previous work [33] for developing an artificial neural network (ANN)-based energy reconstruction procedure for the TACTIC telescope. As the present work employs the same energy reconstruction procedure, we use the above-mentioned cuts only in this work.

A well-established procedure to extract the γ-ray signal from the cosmic-ray background using single imaging telescope is to plot the frequency distribution of α-parameter (defined as the the angle between the major axis of the image and the line between the image centroid and camera centre) of shape and DISTANCE selected events. This distribution is expected to be flat for the isotropic background of cosmic events and for γ-rays, coming from a point source, the distribution is expected to show a peak at smaller α values [20,25–30]. Defining $\alpha \leq 18^\circ$ as the γ-ray domain and $27^\circ \leq \alpha \leq 81^\circ$ as the background

region, the number of γ-ray events is then calculated by subtracting the expected number of background events (calculated on the basis of background region) from the γ-ray domain events. The reason for not including the α bin 18°–27° in the background region is to ensure that the background level is not overestimated because of a possible spill-over of γ-ray events beyond 18°. Since the truncation of the Cherenkov images recorded at the boundary of the imaging camera can distort the flat nature of α-plot for cosmic rays [34] especially when α-parameter is close to ∼90°, the α bin 81°–90° is also excluded while calculating the expected number of background events in the γ-ray domain. Estimating the expected background level in the γ-domain by following this approach is well known [34] and has been used quite extensively by other groups when equal amount of off-source data is not available. However, we have also validated this method for the TACTIC telescope by using separate off-source data on a regular basis [20,25–30] and the α distribution of these data in the range $\alpha \leq 81°$ is in good agreement with the expected flat distribution. The significance of the excess events has been finally calculated by using the maximum likelihood ratio method of Li and Ma [35].

The number of γ-ray events, obtained for each spell along with their statistical significance, after applying the above cuts, are presented in table 3. The corresponding α-plots for the four spells are shown in figures 3a, 3b, 3c and 3d. As a representative example for comparison, α-plots for ∼67.73 h and ∼39.22 h of off-source observations for the data spells OFF-0304 and OFF-0708, respectively are shown in figures 4a and 4b to demonstrate the flat nature of these plots in the absence of a γ-ray signal (identified by the number of excess events in the γ-ray domain with $\alpha \leq 18°$).

Referring back to figures 3a and 3d, one can clearly see evidence of a γ-ray signal when dynamic supercuts are applied to the data. The number of γ-ray events for the four spells are determined to be ∼(979±97), ∼(928±101), ∼(968±90) and ∼(867±96) with corresponding statistical significances of ∼10.3σ, ∼9.4σ, ∼11.1σ and ∼9.2σ, respectively. The resulting γ-ray rates for the four on-source data spells turn out to ∼(9.38±0.93) h^{-1}, ∼(9.40±1.00) h^{-1}, ∼(9.21±0.86) h^{-1} and ∼(9.47±1.05) h^{-1}, respectively. The values of χ^2/DOF for the background region (defined by $27° \leq \alpha \leq 81°$) and the corresponding probability (indicated by columns 5 and 6 respectively in table 3) is also consistent with the assumption that the background region is flat and thus can be reliably used for estimating the background level in the γ-domain. The values of χ^2/DOF for the two off-source α-plots (shown in figure 4) are found to be ∼2.15/5 and ∼7.20/5. With corresponding probabilities of ∼0.828 and ∼0.206, respectively the results are found to be consistent with the assumption that the background region is flat.

Table 3. Detailed spell-wise analysis report of Crab data.

Spell	Obs. time (h)	γ-ray events	γ-ray rate (h^{-1})	Significance (σ)	χ^2/DOF ($27° \leq \alpha \leq 81°$)	Prob.
ON-0304	104.28	979±97	9.38±0.93	10.3	4.92/5	0.426
ON-0506	101.04	928±101	9.40±1.00	9.4	7.11/5	0.213
ON-0708	105.16	968±90	9.21±0.86	11.1	8.02/5	0.155
ON-0910	91.50	867±96	9.47±1.05	9.2	1.21/5	0.944
All data	401.98	3742±192	9.31±0.48	19.9	5.57/5	0.350

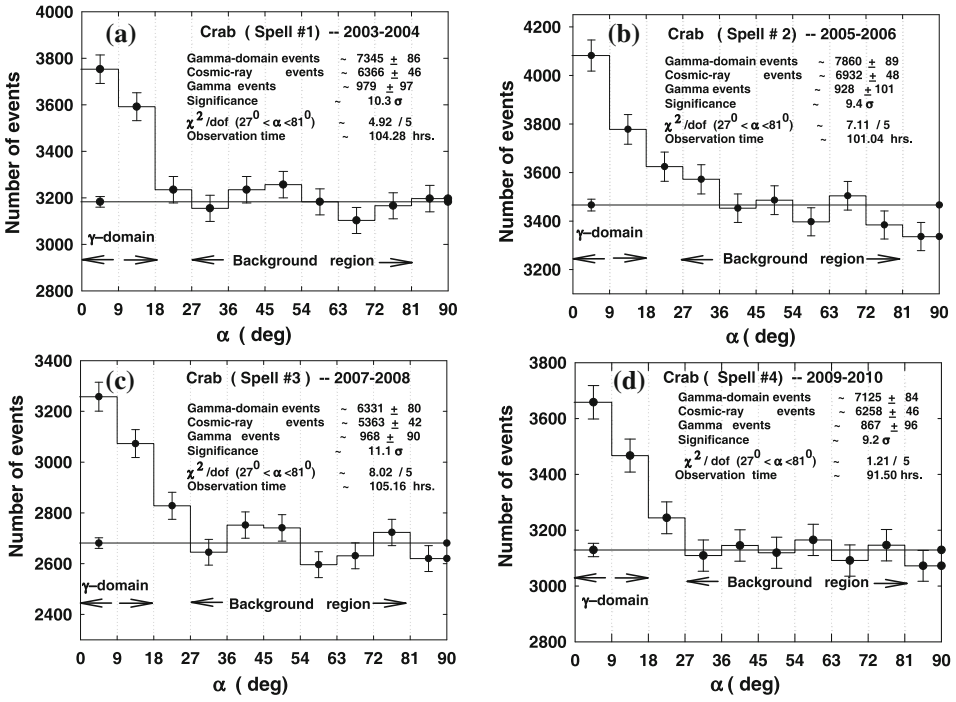

Figure 3. (**a**) Alpha plot for the Crab Nebula when ON-0304 on-source data is analysed. (**b**), (**c**) and (**d**) are same as (**a**) except for the ON-0506, ON-0708 and ON-0910 on-source data spells.

The consolidated on-source α-plot for all the spells taken together is shown in figure 5a. The total data yield an excess of $\sim$(3742$\pm$192) γ-ray events with a statistical significance of $\sim$19.9σ. The resulting γ-ray rate turns out to be $\sim$(9.31$\pm$0.48) h^{-1}. The value of χ^2/DOF $\sim$ 5.57/5 for the background region with the corresponding probability of $\sim$0.35 is again consistent with the assumption that the background region is flat. The cumulative significance level and the number of γ-ray events detected from the Crab Nebula as a function of the observation time is shown in figures 5b and 5c, respectively. The results shown are obtained by cumulatively adding data for one observation night at a time. The main aim of presenting these plots is to validate that the observed excess events are indeed genuine γ-rays from the source. On the basis of these results one can confidently say that the TACTIC telescope has consistently detected γ-ray emission from the 'standard candle' Crab Nebula during the four observations spells at a sensitivity level $N_\sigma \sim 1.0\sqrt{T}$, where T is the observation time in hours. The corresponding number of γ-rays recorded is seen to follow $N_\gamma \sim 9.2$ T.

5. Energy spectrum of the Crab Nebula

Keeping in view the fact that the Cherenkov light emitted from the electromagnetic cascade is to a first-order approximation proportional to the energy of the primary γ-ray, the approach followed in atmospheric Cherenkov imaging telescopes is to determine

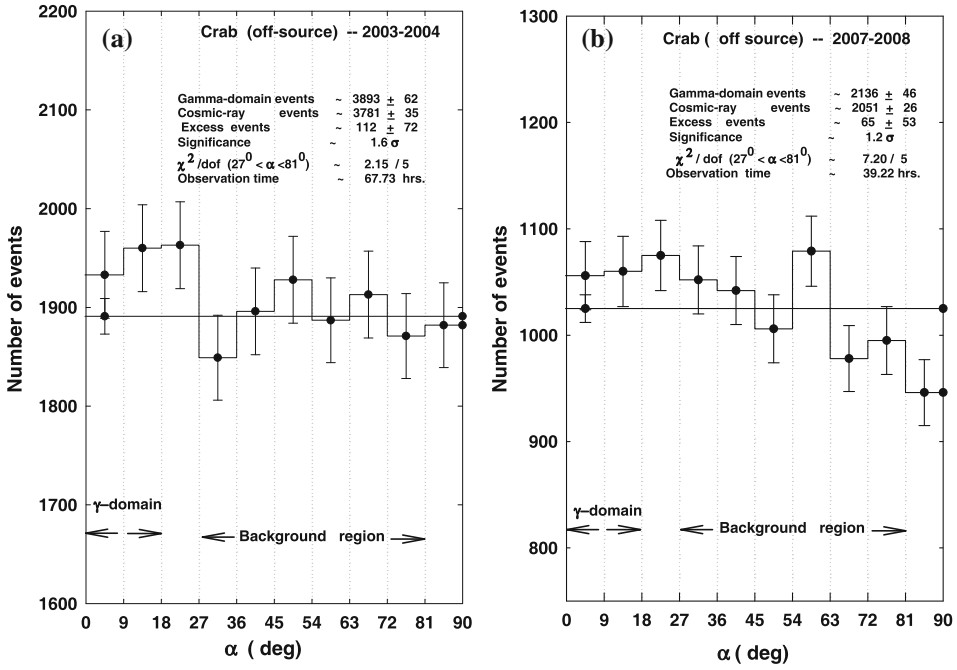

Figure 4. Off-source α-plots for the (**a**) OFF-0304 data spell and (**b**) OFF-0708 data spell.

the energy on the basis of the image SIZE. Since the intensity of the Cherenkov light is a function of core distance, which is not possible to obtain with a single imaging telescope, the angular distance of the image centroid from the camera centre (known as the DISTANCE parameter) is generally used as an approximate measure of the impact distance. The energy reconstruction procedure with a single imaging telescope thus involves using SIZE and DISTANCE parameters of the Cherenkov event for determining energy of the primary γ-ray. Although the method has been found to work reasonably well over a restricted zenith angle range of $\leq 30°$, there is a need to include zenith angle dependence in the energy reconstruction procedure for allowing data collection over a much wider zenith angle range. A novel energy reconstruction procedure, based on the utilization of ANN, has been developed for the TACTIC telescope. While the details of the energy reconstruction procedure can be seen in [33], brief details regarding its implementation and performance evaluation are given below.

Given the inherent power of artificial neural network to effectively handle the multivariate data fitting, we have developed an ANN-based energy estimation procedure for determining the energy of the primary γ-ray on the basis of its image SIZE, DISTANCE and zenith angle. The procedure followed by us uses a 3 : 30 : 1 (i.e 3 nodes in the input layer, 30 nodes in hidden layer and 1 node in the output layer) configuration of the ANN with resilient back propagation training algorithm to estimate the energy of a γ-ray event on the basis of its image SIZE, DISTANCE and zenith angle. The three nodes in the input

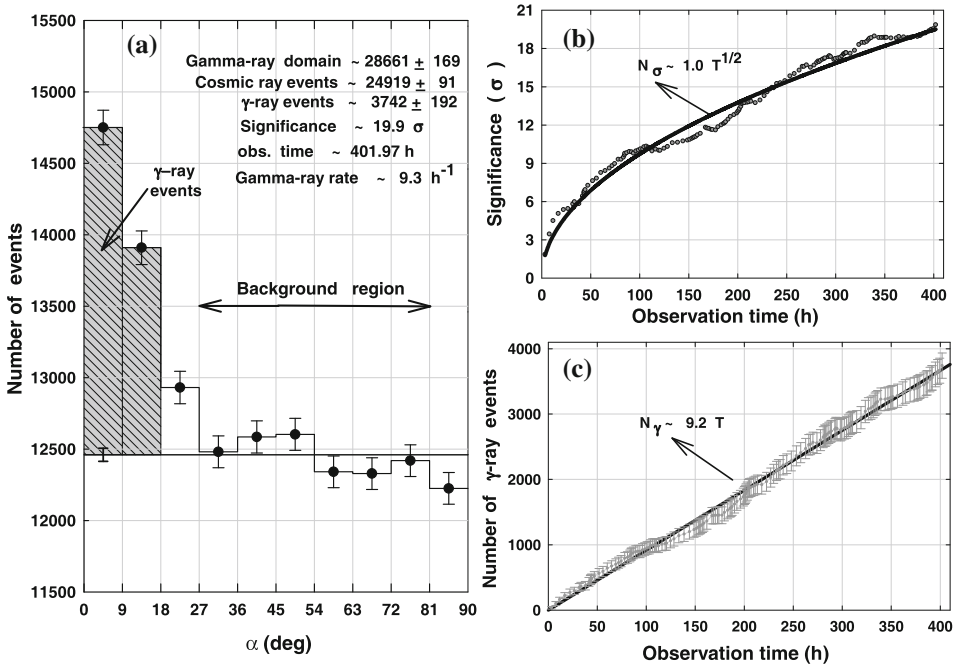

Figure 5. (**a**) On-source α-plot for the Crab Nebula when all the data are analysed, (**b**) cumulative significance level as a function of observation time and (**c**) cumulative number of γ-rays as a function of observation time.

layer correspond to zenith angle, SIZE and DISTANCE, while the one node in the output layer represents the expected energy (in TeV) of the event. The activation function chosen is the sigmoid function.

The performance of the ANN-based energy reconstruction procedure has been evaluated by calculating the relative error in the reconstructed energy (Δ_{E}), for individual γ-ray events using the test data file. The relative error in the reconstructed energy is defined as $(E_{\mathrm{estm}} - E_{\mathrm{true}})/E_{\mathrm{true}}$, where E_{true} is the true energy and E_{estm} is the estimated energy yielded by the energy reconstruction procedure. The mean value of (Δ_{E}) as a function of E_{true} and energy resolution ($\sigma(\Delta_{\mathrm{E}})$) defined as the root mean square width of the distribution of Δ_{E} are the main quantities which can be used for estimating the performance of energy reconstruction procedures [33]. The rms width of the best-fit Gaussian distribution for the test and validation data are found to yield $\sim$22% and $\sim$26%, respectively, with a negligible bias in the energy. Taking higher of the two $\sigma(\Delta_{\mathrm{E}})$ values (i.e $\sigma(\Delta_{\mathrm{E}}) \sim 26\%$) as a safe value of the energy resolution achieved by the ANN-based energy reconstruction procedure, one can safely say that the proposed method, apart from yielding a comparable performance to that of other single imaging telescopes of $\sim$25%, has the added advantage that it considers zenith angle dependence of SIZE and DISTANCE parameters as well. The procedure thus allows data collection over a much wider zenith angle range as against a coverage of up to 30° in case the zenith angle dependence is to be ignored.

The differential photon flux per energy bin has been computed using the formula

$$\frac{\mathrm{d}\Phi}{\mathrm{d}E}(E_i) = \frac{\Delta N_i}{\Delta E_i \sum_{j=1}^{5} A_{i,j}\eta_{i,j}T_j}, \tag{1}$$

where ΔN_i and $\mathrm{d}\Phi(E_i)/\mathrm{d}E$ are the number of events and the differential flux at energy E_i, measured in the ith energy bin ΔE_i and over the zenith angle range of 0°–45°, respectively. T_j is the observation time in the jth zenith angle bin with corresponding energy-dependent effective area ($A_{i,j}$) and γ-ray acceptance ($\eta_{i,j}$). The five zenith angle bins (j=1–5) used are 0°–10°, 10°–20°, 20°–30°, 30°–40° and 40°–50° with effective collection area and γ-ray acceptance values available at 5°, 15°, 25°, 35° and 45°. Dependence of effective collection area as a function of the primary γ-ray for simulated γ-ray showers at zenith angles of 15° and 35° are shown in figures 6a and 6b. While top curves (labelled as Trigger alone) are the effective area when no cuts are applied to the data, the lower curves (labelled as Trigger+DSC) represent when dynamic supercuts analysis methods are applied to the data. The number of γ-ray events (ΔN_i) in a particular energy bin is calculated by subtracting the expected number of background

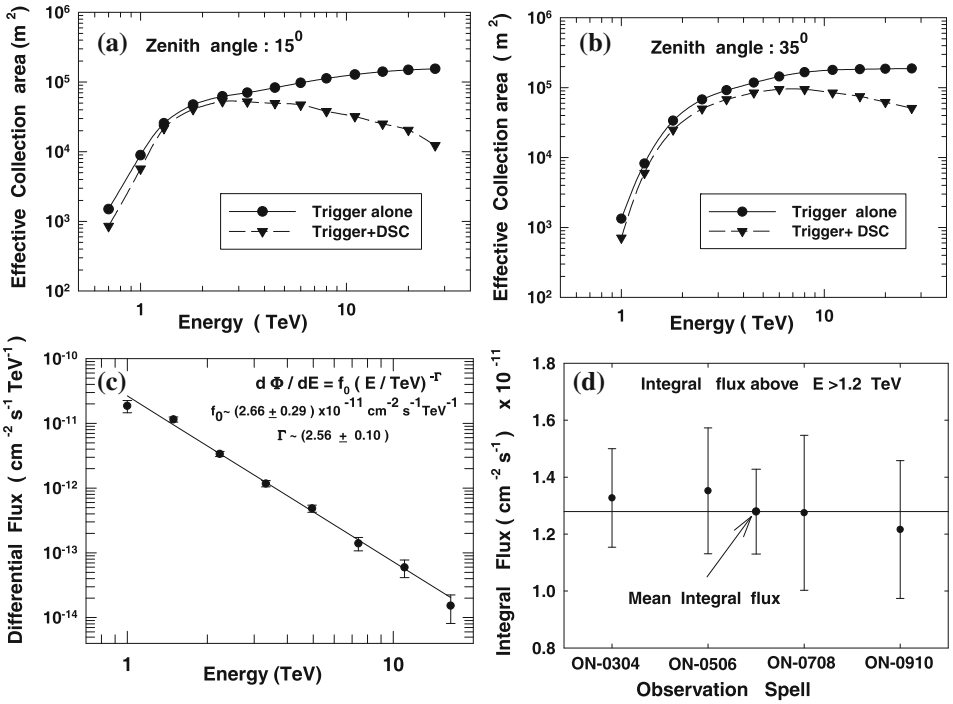

Figure 6. Effective collection area as a function of the primary γ-ray energy for simulated γ-rays at zenith angles of (**a**) 15° and (**b**) 35°. While top curve (labelled as Trigger alone) is the effective area when no cuts are applied to the data, the bottom curve (labelled as Trigger+DSC) represents when dynamic supercuts are applied to the data. (**c**) The differential energy spectrum of the Crab Nebula, as measured by the TACTIC telescope, using the total on-source data of ∼402 h. (**d**) Spell-wise integral flux of γ-rays from the Crab Nebula above ∼1.2 TeV energy.

events, from the γ-ray domain events. After using appropriate values of effective collection area and γ-ray acceptance efficiency (along with their energy and zenith angle dependence) we first determined the γ-ray differential spectrum for each spell separately. The combined spectrum, shown in figure 6c, was then obtained by using inverse square errors as weights for calculating the mean differential flux in each energy bin. Since the data collected by the telescope used two different trigger modes, the above procedure avoids any assumption that the collection areas for the two trigger schemes are same. A power-law fit ($\mathrm{d}\Phi/\mathrm{d}E = f_0 E^{-\Gamma}$) to the measured differential flux data with $f_0 \sim (2.66 \pm 0.29) \times 10^{-11}$ cm^{-2} s^{-1} TeV^{-1} and $\Gamma \sim 2.56 \pm 0.10$ is also shown in figure 6c. The fit has a $\chi^2/\mathrm{DOF} \sim 9.11/6$ with a corresponding probability of ~ 0.17. The errors in the flux constant and the spectral index are standard errors. The spectrum obtained matches reasonably well with that obtained by the Whipple and HEGRA groups [36,37].

The spell-wise integral γ-ray flux from the Crab Nebula above the energy of ~ 1.2 TeV, as measured by the TACTIC telescope, is shown in figure 6d. The flux values for the four on-source data spells (viz., ON-0304, ON-0506, ON-0708 and ON-0910) are found to be $\sim (1.33 \pm 0.17) \times 10^{-11}$ cm^{-2} s^{-1}, $\sim (1.35 \pm 0.22) \times 10^{-11}$ cm^{-2} s^{-1}, $\sim (1.27 \pm 0.27) \times 10^{-11}$ cm^{-2} s^{-1} and $\sim (1.22 \pm 0.24) \times 10^{-11}$ cm^{-2} s^{-1}. The mean integral flux for all the data spells taken together is determined to be $\sim (1.28 \pm 0.15) \times 10^{-11}$ cm^{-2} s^{-1} and is also shown in the figure.

6. Performance evaluation on the basis of sensitivity estimates and guidance for enhancing sensitivity

In this section we shall estimate the sensitivity of the TACTIC telescope. Assuming that main background against which γ-ray signal needs to be detected is due to protons and the detection sensitivity is limited by statistical fluctuations of γ-ray domain events (signal+background) and background region events, the expression for the statistical significance (N_σ), using eq. (9) of Li and Ma [35], is given by

$$N_\sigma = \frac{(N_{\mathrm{on}} - \beta_1 N_{\mathrm{off}})}{\sqrt{\beta_1 (N_{\mathrm{on}} + N_{\mathrm{off}})}} = \frac{(N_\gamma)}{\sqrt{\beta_1 (N_{\mathrm{on}} + N_{\mathrm{off}})}}, \tag{2}$$

where N_{on} is the number of events in the γ-ray domain ($\alpha \leq 18^\circ$), N_{off} is the number of events in the background region ($27^\circ \leq \alpha \leq 81^\circ$) and $\beta_1 (= 2/6)$ is the ratio of γ-ray domain ($\alpha \leq 18^\circ$) to background region ($27^\circ \leq \alpha \leq 81^\circ$). Using the fact that only 60% (denoted by β_2 where $\beta_2 = 0.6$) of the total cosmic-ray events contribute to the α-range of the background region with $27^\circ \leq \alpha \leq 81^\circ$, we get $N_{\mathrm{on}} = N_{\gamma 0} + \beta_1 \beta_2 N_{\mathrm{p0}}$ and $N_{\mathrm{off}} = \beta_2 N_{\mathrm{p0}}$ ($N_{\gamma 0}$ and N_{p0} are the number of γ-ray and cosmic-ray events, respectively without applying any γ-domain cuts).

One of the ways of estimating the sensitivity is to calculate the minimum signal recovery time needed for detecting a γ-ray signal at an adequately high statistical significance (usually $N_\sigma = 5\sigma$ is used as a benchmark in the field). Using the definition of N_σ given in eq. (2), the expression for the minimum signal recovery time (T_{min}) is given by

$$T_{\mathrm{min}} \approx N_\sigma^2 \left[\frac{\beta_1}{R_\gamma} + (\beta_1 (\beta_1 + 1) \beta_2) \frac{R_{\mathrm{p}}}{R_\gamma^2} \right], \tag{3}$$

where R_γ and R_p are the γ-ray and cosmic-ray rates surviving the γ-domain cuts, respectively and these are given by

$$R_\gamma = \int_{E_\mathrm{min}}^{E_\mathrm{max}} \frac{\mathrm{d}F_\gamma}{\mathrm{d}E} A_\gamma(E)\eta_\gamma(E)\mathrm{d}E, \tag{4}$$

$$R_\mathrm{p} = \int_{E_\mathrm{min}}^{E_\mathrm{max}} \frac{\mathrm{d}F_\mathrm{p}}{\mathrm{d}E}\, A_\mathrm{p}(E)\eta_\mathrm{p}(E)\mathrm{d}E, \tag{5}$$

where $\mathrm{d}F_\gamma/\mathrm{d}E \sim 2.79\times10^{-7}(E/1\ \mathrm{TeV})^{-2.57}\ \mathrm{m}^{-2}\ \mathrm{s}^{-1}\ \mathrm{TeV}^{-1}$ is the differential energy spectrum of the Crab Nebula as measured by the HEGRA group [37], A_γ(E) is the effective collection area for γ-rays in m^2, $\mathrm{d}F_\mathrm{p}/\mathrm{d}E \sim 0.096E^{-2.7}\ \mathrm{m}^{-2}\ \mathrm{s}^{-1}\ \mathrm{sr}^{-1}\ \mathrm{TeV}^{-1}$ is the differential energy spectrum of the protons [38], A_p is the effective collection area for protons in units of m^2 sr; and as already defined, η_γ and η_p are the γ-ray and protons acceptance factors, respectively after the application of selection cuts. Although many groups have used quality factor (QF) (where $\mathrm{QF} = \eta_\gamma/\sqrt{\eta_\mathrm{p}}$) for estimating the sensitivity and for optimizing the performance of their classification methods, we shall use T_min for estimating the performance of the telescope. The reason for this is the fact that a high value of QF can also result from tight cut which can reduce the γ-ray retention factor significantly.

It is evident from eq. (3) that the calculation of T_min, for a particular γ-ray source, involves using effective collection areas for γ-rays and cosmic rays and the corresponding retention factors after applying γ-domain cuts. Since all these variables, apart from being energy dependent are also a function of zenith angle, rigorous calculation of T_min, for a particular source, can be performed only if the actual zenith angle coverage is also duly considered in the calculation. While we have accounted for all the above-mentioned dependences in determining the energy spectra of the Crab Nebula, Mrk 421 and Mrk 501 [25–28], useful knowledge about the system performance can also be obtained if the calculations are performed on the basis of simple toy model. In this model, we use typical average values of these quantities so that one can directly find out the expected cosmic-ray and γ-ray rates by multiplying their integral spectra with effective collection areas. With these approximations, expression (3) can be rewritten as

$$T_\mathrm{min} \approx N_\sigma^2 \left[\frac{\beta_1}{R_{\gamma0}\eta_\gamma} + (\beta_1(\beta_1+1)\beta_2)\,\frac{R_\mathrm{p0}\eta_\mathrm{p}}{R_{\gamma0}^2\eta_\gamma^2}\right], \tag{6}$$

where $R_{\gamma0}$ and R_p0 are the γ-ray and cosmic-ray rates without applying any γ-domain cuts, respectively. With $\mathrm{QF} = \eta_\gamma/\sqrt{\eta_\mathrm{p}}$, the above expression can be rewritten as

$$T_\mathrm{min} \approx N_\sigma^2 \left[\frac{\beta_1}{R_{\gamma0}\eta_\gamma} + (\beta_1(\beta_1+1)\beta_2)\,\frac{R_\mathrm{p0}}{R_{\gamma0}^2 QF^2}\right] \tag{7}$$

Following this simplified approach, figure 7 shows the sensitivity of the TACTIC telescope as a function of observed γ-ray rate (i.e. R_γ). The sensitivity plotted in figure 7 is in terms of the signal recovery time for detecting a 5σ steady signal from the Crab Nebula at an energy above ~1.2 TeV and by using $A_\gamma \sim 4\times10^4\ \mathrm{m}^2$. The estimated γ-ray

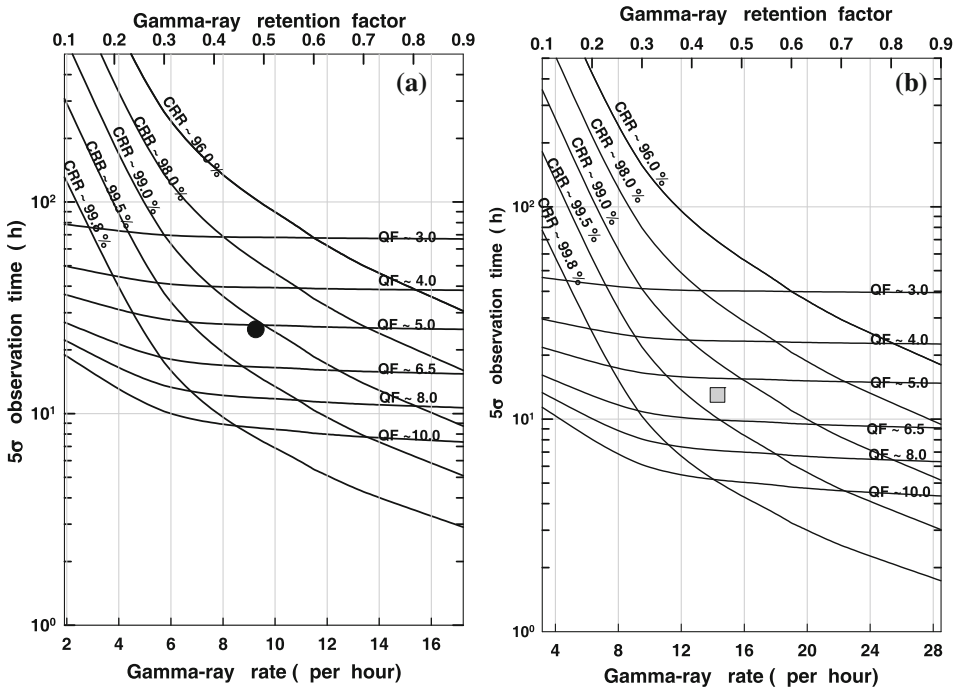

Figure 7. Sensitivity estimate of the TACTIC telescope in terms of the signal recovery time for 5σ steady detection from Crab Nebula as a function of measured γ-ray rate above γ-ray energies of (**a**) 1.2 TeV and (**b**) 0.8 TeV. Several representative curves obtained for different values of η_p and QF are also shown in the figure.

rate without applying any γ-domain cuts is found to be $\sim$19.1 h^{-1}. The corresponding γ-ray retention values are also shown at the top of the figure so that one can estimate the γ-ray retention factor on the basis of the measured γ-ray rate. In order to estimate the cosmic-ray rate while one can follow a similar procedure, by using appropriate values of relevant parameters, the resulting predicted rate can be somewhat underestimated because of additional contribution of $\sim$30% to the measured event rate due to other cosmic-ray nuclei [38]. While we have accounted for this appropriately in our detailed simulation work [24], for the simplified approach followed here, one can directly use a value of R_{p0} $\sim$1.8 Hz for estimating the cosmic-ray rejection capability of the telescope. This value is obtained by taking the mean of observed cosmic-ray rates for the NN-2 and NN-3 trigger rates observed at a typical zenith angle of $\sim$20°.

On examining figure 7a, it is evident that sensitivity level of $\sim 5.0\sigma$ in $\sim$25 h (shown as filled circle in the figure) corresponds to $\eta_\gamma \sim 0.50$ and $\eta_p \sim 0.0093$ (i.e. cosmic-ray rejection $\sim$99.07%). Several representative curves obtained for different values of η_p and QF are also shown in the figure so that useful guidance can be obtained from this figure for improving the sensitivity.

The efficiency of the dynamic supercuts is also found to be biased towards lower energies and this can also be seen in figures 6a and 6b. This is the main reason because of

which we are unable to determine the Crab Nebula energy spectrum beyond 16.5 TeV. In order to obviate this problem, we have also studied the performance of the Levenberg–Marquardt ANN algorithm for gamma/hadron segregation and the method yields very encouraging results when applied to the ON-0506 Crab Nebula data [39]. Superior performance of Lavenberg–Marquardt-based ANN network has enabled us to retain relatively higher number of events at energies above ∼9 TeV as compared to the dynamic supercuts procedure [39].

Figure 7b shows how $T_{\min}$ varies with observed γ-ray rate when the calculations are performed at γ-ray energies above 0.8 TeV. This figure clearly reveals that a $\sim 5\sigma$ detection in an observation period of ∼13 h can be achieved if the γ-ray energy threshold is reduced to $E_\gamma \sim 0.8$ TeV. This has been already achieved in Dec. 2011 by installing new compound parabolic concentrators and a brief summary of the upgradation work is presented in the next section of this work. It is also evident from figure 7b that to a sensitivity level of $\sim 5\sigma$ detection in ∼5 h at $E_\gamma \sim 0.8$ TeV, we need a cosmic-ray rejection of ∼99.5% and γ-ray acceptance of ∼0.7.

7. Recent upgradation and the road ahead

Major upgrading work, involving replacement of signal and high voltage cables and installation of new compound parabolic concentrators was taken up in Nov.–Dec. 2011 for improving the sensitivity of the telescope. While detailed simulation and experimental results, after upgradation are still under preparation, we shall present here only a brief summary of the upgradation work and some 'quick look' results. New compound parabolic concentrators with square entry and circular exit aperture were installed on the TACTIC imaging camera in order to increase its photon collection efficiency. The reflection coefficient of the new CPCs was measured to be ∼85% in the wavelength range 400–550 nm. Apart from removing the dead space in between the PMTs completely, use of the new CPCs has also helped us to improve the gamma/hadron segregation capability of the telescope. In addition, the trigger criteria were also modified by including more nearest-neighbour collinear triplet combinations. A dedicated CCD camera was also installed for conducting detailed point run calibrations and data collected have been successfully used for determining the position of the source in the image plane with an accuracy of better than $\sim\pm 3$ arc-min. The analysis procedure has also been upgraded by using the ASYMMETRY parameter [40] so that additional 40% of the hadronic background can be further removed by identifying the 'head' and 'tail' feature of Cherenkov images. The ASYMMETRY parameter gives a measure of the skewness of the Cherenkov light distribution relative to the image centroid and is equal to $\sqrt[3]{\sigma'_{x^3}}$/LENGTH, where σ'_{x^3} is the third-order moment of the image along the major axis. It is worth mentioning here that the γ-ray images have their head closer to the assumed source position in the imaging camera and thus can be selected preferentially demanding a positive value for the ASYMMETRY parameter. Analysis of the ∼27 h data collected with the telescope between 23 Dec. 2011 and 29 Dec. 2011, after completing the hardware and software upgrading work, yields an increase in the prompt coincidence rate from ∼2.4 Hz (at zenith angle of 0°0) to ∼3.8 Hz. This translates to reduction in the threshold energy of the telescope for cosmic rays from ∼1.8

TeV to ∼1.4 TeV and from ∼1.2 TeV to ∼0.8 TeV for the γ-rays. Detailed simulation studies are in progress to confirm these estimates. As a result of the upgradation and more refined data analysis, the sensitivity of the TACTIC telescope has improved from $N_\sigma \sim 1.0\sqrt{T}$ to $N_\sigma \sim 1.4\sqrt{T}$. The γ-ray rate per hour from the Crab Nebula has also increased from ∼9.2 to ∼14.3. The telescope can now detect the TeV γ-ray emission from the Crab Nebula at $\sim 5\sigma$ in an observation period of ∼13 h as compared to ∼25 h earlier.

We have also studied the gamma/hadron segregation potential of various ANN algorithms for the TACTIC telescope, by applying them to the Monte Carlo simulated and the ON-0506 data spell on the Crab Nebula. Application of Levenberg–Marquardt ANN algorithm to this data spell yields an excess of $\sim(1141\pm106)$ with a statistical significance of $\sim 11.1\sigma$, as against an excess of $\sim(928\pm100)$ with a statistical significance of $\sim 9.4\sigma$ obtained with dynamic supercut selection methodology. The main advantage accruing from the ANN methodology is that it is more effective at higher energies and this has allowed us to re-determine the Crab Nebula energy spectrum in the energy range ∼1–24 TeV [39].

In the end, it is worth having a closer look at some of the scientific drivers which motivate observations in the multi-TeV energy range with a dedicated instrument like TACTIC. With ever growing number of γ-ray sources in the sky and rather limited field of view of Chernkov imaging telescopes, most of the TeV sky remains relatively unexplored and only 10% of the sky has been observed so far. Searching for γ-ray emission from different types of blazars including high-energy peaked BL Lac objects (HBLs), intermediate energy peaked BL Lac objects (IBLs), and flat spectrum radio quasars (FSRQs) is an important research field where we can also contribute to understand the γ-ray emission characteristics in different types of blazars. The most notable observational results from the blazars have been extremely fast large amplitude flux and spectral variability on hour time-scales, and a pronounced X-ray TeV γ-ray flux correlation. Studying the temporal correlation between flux variations at different wavelengths during flares can help in providing constraints on the blazar emission models. While multiwavelength information, in particular at radio and X-ray energies, can provide constraints on hadronic or leptonic components, one often requires model-dependent assumptions to decide the nature of the parent particles.

One of the objectives of the TACTIC telescope will be to conduct deep observations on a small number of well-known VHE blazars like Mrk 421, Mrk 501, H1426+428, 1ES1959+650, BL Lacertae and 1ES 2344+514. In this regard, it is quite reassuring to find that the energy spectrum of the Mrk421 measured by the TACTIC telescope, for the data collected between 27 December 2005 and 07 Feb. 2006, has been used in [41] while interpreting the results of the Swift observations between April 2006 and July 2006. Participating in target of opportunity observations of flaring blazars is another important area where results from the TACTIC telescope can help in constraining the blazar emission models. Further, the TeV energy spectra of extragalactic sources also carry the imprint of extragalactic absorption in the form of 'characteristic high-energy cut-offs' at energies above 100 GeV energy range. Detecting this imprint of absorption thus is yet another scientific objective where results from TACTIC telescope can be useful by providing deep observations of blazars and by determining their energy spectra with good accuracy.

8. Conclusions

The TACTIC imaging telescope has been in operation at Mt. Abu since 2001 and has so far detected γ-ray emission from the Crab Nebula, Mrk 421 and Mrk 501. Over the years there has been reasonably good matching of the Crab Nebula spectrum with that obtained by other groups. Apart from validating the stability of the TACTIC subsystems directly with γ-rays from this source, matching of the Crab Nebula spectrum also validates the full analysis chain, including the inputs used from the Monte Carlo simulations, like, effective area and γ-ray acceptance factors and the energy reconstruction procedure. With an enhanced sensitivity of $N_\sigma \sim 1.4\sqrt{T}$ after upgradation, there is considerable scope for the TACTIC telescope to monitor TeV γ-ray emission activity from various active galactic nuclei on a long term basis. Participating in multiwavelength observation campaigns on various active galactic nuclei and determining the energy spectrum of these sources (both at low average flux levels of < 1 crab unit and from intense flares of >2 crab units) will be one of the main scientific objectives for which the TACTIC telescope will be used during the next few years. The data collected on these sources will also be utilized to understand the γ-ray production mechanisms of these objects and absorption effects at the source or in the intergalactic medium due to interaction of γ-rays with the extragalactic background photons.

Acknowledgements

The authors would like to thank colleagues at the Centre for Design and Manufacture, the Electronics Division and Astrophysical Sciences Division of BARC who have contributed during the various stages of the planning, fabrication, installation and operation of the telescope. They would also like to thank the anonymous referee for making several helpful suggestions.

References

[1] J Holder, *Astropart. Phys.* **39–40**, 61 (2012)
[2] F Aharonian *et al*, *Rep. Prog. Phys.* **71**, 096901 (2008)
[3] P M Chadwick *et al*, *J. Phys. G: Nucl. Part. Phys.* **35**, 033201 (2008)
[4] F W Stecker and O C De Jager, *Ap. J.* **476**, 712 (1997)
[5] E Dwek and F Krennrich, *Ap. J.* **618**, 657 (2005)
[6] F Aharonian *et al*, *Nature* **440**, 1018 (1989)
[7] T C Weekes *et al*, *Ap. J.* **342**, 379 (1989)
[8] A Daum *et al*, *Astropart. Phys.* **8**, 1 (1997)
[9] A M Hillas, *Proc. 19th ICRC, La Jolla* **3**, 445 (1985)
[10] D J Fegan, *Space Sci. Rev.* **75**, 137 (1996)
[11] G Mohanty *et al*, *Astropart. Phys.* **9**, 15 (1998)
[12] J A Hinton *et al*, *New Astron. Rev.* **48**, 331 (2004)
[13] O C de Jager *et al*, *Ap. J.* **457**, 253 (1996)
[14] J Aleksic *et al*, *Ap. J.* **742**, 42 (2011)
[15] E Aliu *et al*, *Science* **334**, 69 (2011)
[16] A A Abdo *et al*, *Science* **331**, 739 (2011)

[17] R Ojha *et al*, *ATel 4855* (2013)
[18] G Aielli *et al*, *ATel 2921* (2010)
[19] B Bartoli *et al*, *ATel 4258* (2012)
[20] R Koul *et al*, *Nucl. Instrum. Methods A* **578**, 548 (2007)
[21] A K Tickoo *et al*, *Nucl. Instrum. Methods A* **539**, 177 (2005)
[22] S R Kaul *et al*, *Nucl. Instrum. Methods A* **496**, 400 (2003)
[23] K K Yadav *et al*, *Nucl. Instrum. Methods A* **527**, 411 (2004)
[24] M K Koul *et al*, *Nucl. Instrum. Methods A* **646**, 204 (2011)
[25] K K Yadav *et al*, *Astropart. Phys.* **27**, 447 (2007)
[26] P Chandra *et al*, *J. Phys. G: Nucl. Part. Phys.* **37**, 125201 (2010)
[27] P Chandra *et al*, *J. Phys. G: Nucl. Part. Phys.* **39**, 045201 (2012)
[28] S V Godambe *et al*, *J. Phys. G: Nucl. Part. Phys.* **35**, 065202 (2008)
[29] S V Godambe *et al*, *J. Phys. G: Nucl. Part. Phys.* **34**, 1683 (2007)
[30] K K Yadav *et al*, *J. Phys. G: Nucl. Part. Phys.* **36**, 085201 (2009)
[31] R J Protheroe *et al*, *Proc. 25th ICRC, Kruger Park, South Africa* **8**, 317 (1997)
[32] A Konopelko, *Astropart. Phys.* **24**, 191 (2005)
[33] V K Dhar *et al*, *Nucl. Instrum. Methods A* **606**, 795 (2009)
[34] M Catanese *et al*, *Ap. J.* **501**, 616 (1998)
[35] T P Li and Y Q Ma, *Ap. J.* **272**, 317 (1983)
[36] A M Hillas *et al*, *Ap. J.* **503**, 744 (1998)
[37] F Aharonian *et al*, *Ap. J.* **614**, 897 (2004)
[38] A Konopelko, *Astropart. Phys.* **24**, 191 (2005)
[39] V K Dhar *et al*, *Nucl. Instrum. Methods A* **708**, 56 (2013)
[40] D J Fegan, *J. Phys. G: Nucl. Part. Phys.* **23**, 1013 (1997)
[41] A Tramacere *et al*, *Astron. Astrophys. A* **501**, 879 (2009)